IEEE Access
Multidisciplinary ⋮ Rapid Review ⋮ Open Access Journal

Received 3 January 2024, accepted 15 January 2024, date of publication 30 January 2024, date of current version 16 February 2024.

Digital Object Identifier 10.1109/ACCESS.2024.3360213

RESEARCH ARTICLE

A New Traction System With Asymmetrical Six-Phase Permanent Magnet Synchronous Motors for Hydrogen Trains

NURSAID POLATER[1], FRANCESCO MAGGIULLI[2], GIOVANNI MARIA FOGLIA[2], AND PIETRO TRICOLI[3], (Senior Member, IEEE)

[1]Department of Electrical and Electronics Engineering, Faculty of Engineering and Architecture, Yozgat Bozok University, 66200 Yozgat, Turkey
[2]Department of Energy, Politecnico di Milano, 20156 Milan, Italy
[3]Department of Electronic, Electrical and Systems Engineering, University of Birmingham, B15 2TT Birmingham, U.K.

Corresponding author: Nursaid Polater (nursaid.polater@bozok.edu.tr)

This work was supported in part by the Ministry of National Education, Republic of Türkiye, for doctoral studies of Nursaid Polater at the University of Birmingham, through the Scholarship of Higher Education, under Grant 64243970/150.02/8603043; and in part by Politecnico di Milano, Italy, through the Scholarship for a thesis abroad of Francesco Maggiulli.

ABSTRACT This paper proposes a new traction system with asymmetrical six-phase permanent magnet synchronous motors to replace traditional induction and permanent magnet machines for hydrogen trains. The main benefit of the proposed traction system is the elimination of the boost converters of the fuel cells (FCs) and the battery. The proposed traction system has two three-phase inverters feeding separately the six-phase machine and controlled to achieve optimal power sharing between the FC and the battery. The model of the system and its control has been implemented on a micro-controller and validated with a hardware-in-the-loop simulator. A comparison of the proposed topology with traditional motor drives has shown a mass reduction of 85% and a volume reduction of around 14% for basic components. Therefore, the proposed traction configuration and power-sharing strategy is a very interesting candidate for hydrogen trains.

INDEX TERMS AS-PMSM, fuel cell (FC), Li-ion battery cells, traction power converter.

NOMENCLATURE

ASPMSM	Asymmetrical six-phase permanent magnet synchronous motor.
PMSM	Permanent magnet synchronous machine.
T-NPC	T-type neutral point clamped.
DC	Direct current.
AC	Alternating current.
ACH	Always charging.
DEC	Deceleration.
ACC	Acceleration.
CRUISE	Cruising.
SOC	State of Charge.
HIL	hardware-in-the-loop.
FOC	Field oriented control.
STS	Single train simulator.
FC	Fuel cell.
APD	Anti-parallel diode.

The associate editor coordinating the review of this manuscript and approving it for publication was Sze Sing Lee.

I. INTRODUCTION

Governments around the world are taking efforts to decarbonise railway transport by phasing out diesel trains in favour of cleaner alternatives. Despite the expansion of railway electrification programmes, it is unlikely that all routes will be electrified, because the high capital of the infrastructure will not justify the business case for less busy lines. Therefore, it is expected that these lines will use hybrid-electric trains, with a combination of hydrogen FCs and batteries. Battery-only trains will likely to be used for shorter journeys, whereas batteries and FCs will be preferred for longer routes or higher speed services.

Railway traction systems will need to be modified to accommodate these novel power sources. In the current state-of-the-art, FCs and batteries are connected to the traction drive via DC/DC converters [1], [2], [3] as the block diagram is shown in **Fig. 1**. The DC/DC converter of the FC must be unidirectional to avoid negative current circulation, while the DC/DC converter of the battery must be bidirectional to enable charging and discharging operations [4]. The research on traction systems for hydrogen trains has mainly focused on three aspects: increasing the voltage boost ratio of DC/DC converters, increasing the power density of DC/DC converters, and increasing the power density of traction motors.

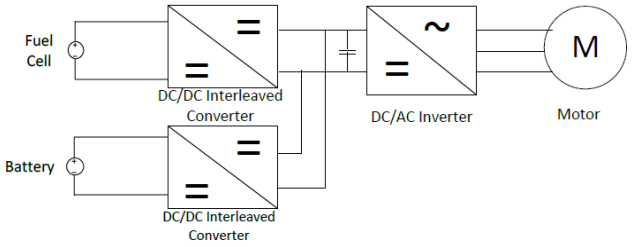

FIGURE 1. Block diagram of conventional traction scheme.

With reference to the first aspect, four phases interleaved boost converters enable to boost the voltage with a ratio of 4:1, with lower ripples of the input and output voltages compared to basic topologies [5], [6], [7], [8]. Additional characteristics, such as fast-dynamic control which respects the integrity of each source while fulfilling the load's rapid power requirements, are required to enable fast transition from traction to regenerative braking [9], [10].

With reference to the second aspect, one of the main drawbacks of using DC-DC converters is the presence of a large inductor to boost the voltage to the desired level. DC-DC converters comprise inductors and capacitors to temporarily store the energy required for the power conversion and they can take up half of the space within a converter [11], [12], [13], albeit the size of energy storage can be reduced using interleaving [14]. Interleaved converters have been proposed for high-power applications due to the smoothness of the battery current [15] higher power density compared to standard boost DC/DC converters, better thermal capabilities, reduced current stresses of power semiconductors, and higher efficiency [15]. Interleaved converters are mostly used in traction systems where high current is required [16]. Also, a multi-source converter topology has been proposed in [17] to enable the connection of several DC sources including FCs, batteries, and supercapacitor banks without inductors. Also, the motor can be operated directly from energy storage units without boosting its voltage with DC/DC converters, increasing the overall conversion efficiency [18]. However, an independent control of the motor and the sources is not possible for all the operating conditions and hence some sources are forced to be charged and discharged on the basis of the motor demand. Also, regenerative braking operations are limited by the actual voltage of the sources.

Boost-inverters have been introduced to combine both boosting and DC/AC power conversion in a single stage. This design uses two identical bidirectional boost converters and has higher conversion efficiency and lower converter size and cost. However, control complexity is moderately high for boost-inverters [19]. With reference to the third aspect, several previous works have extensively demonstrated the advantages of permanent magnet synchronous motors (PMSM) for railway traction systems [20] [21] [22], albeit the industrial uptake has been so far limited due to the need of individual traction inverters. For hydrogen trains, comparisons between induction motors and PMSMs with multiphase windings have shown that in the latter the electrical power can be shared efficiently between phases and could provide tolerance against phase failure, and do not have rotor losses [23].

Six-phase PMSMs are classified based on the phase displacement angle [24] and number of neutral point for each phase group [25]. Amongst the multiphase PMSMs, an asymmetrical six-phase PMSM (AS-PMSM) which has 30° displacement angle, have been proposed for concept designs of traction systems due to their advantages, such as the reduction of fifth and seventh input voltage harmonics, which enables better voltage management and effective voltage utilisation of the inverter because there is no zero sequence element [26]; fault tolerance through the use of a single neutral connection [26], and higher smoothness and stability of the torque [27].

The multiphase/multi-three phase system also facilitates the motor coils' electrical and magnetic isolation, preventing the interaction between the two or three phases in the event of a breakdown. This means that a single-phase outage does not affect the system [28]. In this regard, [29] provides a simple analysis regarding fault tolerant converter topologies that ought to be rearranged for the multiphase structures to increase the system reliability. Since fault-tolerant T-type neutral point clamped (T-NPC)s have a wider level of freedom for switching cases, they allow fault-free operation. T-NPCs with three levels exhibit excellent harmonic distortion performance and efficiency, as well as low common-mode voltage and electromagnetic interference (EMI) and great reliability [29]. D-NPC, two- and three-level converters [30], [31] can also be called fault-tolerant power-conditioning equipment, in addition to T-NPC converters with AS-PMSM could be useful for the proposed architecture.

Nevertheless, multiphase motors have several limitations, namely the inability to establish an air-gap flux at some of the stator current harmonics [32]. The stator resistance (Rs) and leakage inductance restrict all of these harmonics (Ls). Furthermore, these harmonics can arise in almost any voltage excitation caused by a low-impedance current route, in which the current flows with little resistance regardless of whether the current is ordinary or faulty [33].

It should be highlighted that back EMF leads to harmonic distortion in PMSMs [34] [35] [36], and that the torque ripple increases in proportion to the magnitude of the harmonic components. A comparative study of three and six-phase PMSMs can be found in [28]. Although the major criterion for traction motors is that they require less maintenance, recent research has concentrated on improving traction motor efficiency. Therefore designers used induction motors to save money on maintenance, but PMSMs are more efficient. Reference [21] investigated and tested totally enclosed self-cooled PMSMs for narrow gauge trains in order to meet the efficiency aim of PMSMs as well as [38] investigates the effects of paralleling motors for multi-motor traction system.

In this paper, two of the three main problems of traction systems for hydrogen trains have been addressed with a completely different approach based on a AS-PMSM fed by the FC and the battery via two independent inverters. Those two contributions are given below.

The primary contribution of this study is the conceptual design of a traction system with AS-PMSM applied to a regional hydrogen train to replace a diesel train operating in the UK and removal of DC to DC conversion step as the block scheme is given in **Fig. 2**. The paper proposes an optimal power split control according to the operating modes of the train and the state of charge SOC of the battery. The control system uses the motor itself as a means of transferring energy from the FC to the battery via the airgap flux linkage. Also, regenerative braking is controlled to charge the battery.

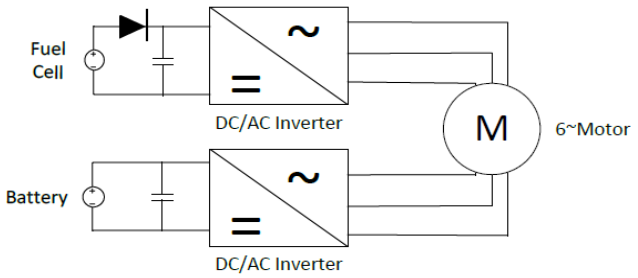

FIGURE 2. Block diagram of proposed traction scheme.

This article is structured as follows. Section II discusses the strategy to split the traction power between FCs and batteries. In section III, the traction system components have been designed with the single train simulator of the University of Birmingham. Then the new traction system has been validated for a realistic case study in Section IV with hardware in the loop implementation. Section V compares the proposed traction system with a traditional system with DC/DC converters. Finally, conclusion remarks are given in section VI.

II. TRACTION PROPULSION UNIT

The proposed configuration of the traction system for hydrogen trains with AS-PMSMs is shown in **Fig. 3**, while the main data of the train and traction system are given in **Table 1** where the *d-q* mutual inductances existed between windings

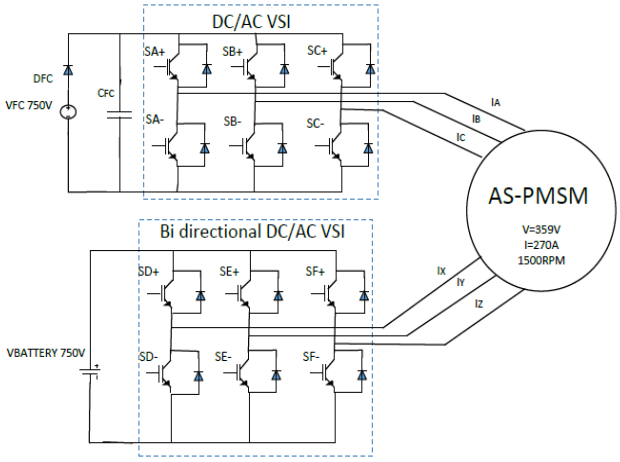

FIGURE 3. Proposed motor drive for hydrogen trains with AS-PMSM.

TABLE 1. Main data of the train, power sources, and traction motors.

Number of carriages per train	4
Number of motors per carriage	2
Train maximum speed [km/h]	48
Train mass [tonne]	147
Wheel radius [m]	0.5
Gearbox ratio of the motor	6
DC-link voltage of original train (V)	750
Rated motor speed [rpm]	1500
Rated motor torque [Nm]	700
Max motor torque for 2 minute [Nm]	850
Nominal motor voltage [V]	359
Nominal motor current [A]	270
Per-phase stator resistance [Ω]	0.008
Direct and quadrature axis' leakage inductances [mH]	5.2
Direct and quadrature axis' mutual inductances [mH]	2.7
Equivalent inertia referred to the motor's axis [kg m^2]	147
FC power [kW]	30
FC voltage, DC/DC Converter Input Voltage [V]	500
FC voltage, DC/AC Inverter Input Voltage [V]	750
Battery power [kW]	90
Battery voltage, DC/DC Converter Input Voltage [V]	500
Battery voltage, DC/AC Inverter Input Voltage [V]	750

sets and *d-q* leakage inductances refer to the windings' self-inductances. This topology uses 2 voltage source inverters directly fed by the FC and the battery without DC-DC boost converters. A dedicated set of 2 inverters is used for each PMSM and each car has two motored axles. The power ratings of the converters depend upon both voltage and current ratings of the DC sources and the motor. The FC converter is designed for the average power of the train, while the battery converter is designed to provide the peak power demand. Therefore, the converters have different ratings that are discussed in detail in section V. Moreover, the FC converter has a series diode to protect the FC against current reversal from the motor drive. Lastly, small capacitors are needed to filter out the high frequency current harmonics of the inverter.

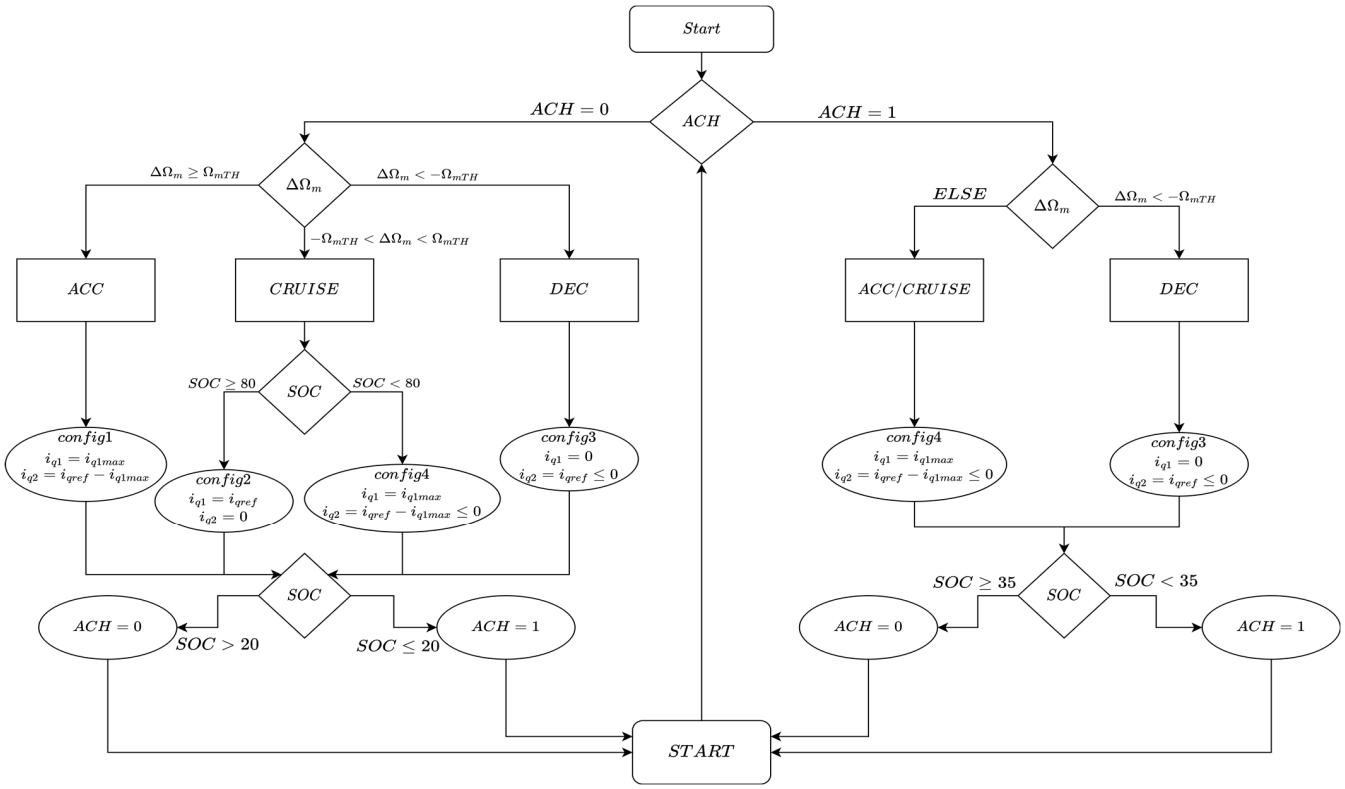

FIGURE 4. Controller flow chart.

The proposed power-sharing scheme takes advantage of the independent control of the 2 power sources. The motor is controlled with a traditional field-oriented vector control with field weakening [39]. The motor torque is controlled by the q-axis current components of the 2 windings, i_{q1} and, i_{q2}, respectively, while the d-axis components are kept to zero up to the base speed and then are decreased to reduce the flux linkage. The existence of two direct axis currents and two quadrature axis currents provides more degrees of freedom compared to a standard three-phase PMSM, such as voltage drop compensation, and also fault tolerant operations when one of the inverters breaks down.

Fig. 4 depicts the flow chart of the control system, where ACH is charging mode (1 for ON and 0 for OFF), ACC is acceleration mode, CRUISE is the cruising mode, DEC is deceleration mode, $\Delta\Omega_m$ is the difference between reference and actual speeds, and Ω_{mTH} is the speed difference threshold. The threshold has been introduced to switch between different operating modes, considering that in reality the speed is never exactly constant. Also, the battery is used in the range 20%-80% of its state of charge (SOC) to reduce degradation effects due to deep cycle and, hence, increase its lifetime.

If the battery's SOC is higher than 20%, ACH is OFF and the FC and the battery operate together. In ACC mode, the maximum q-axis current component of the FC is limited to i_{q1max}. Therefore, if the required q-axis current from the motor i_{qref} is larger than i_{q1max}, the battery will contribute with the difference. In DEC mode, regenerative braking is activated to charge the battery from the kinetic energy of the train. The FC current i_{q1} is set to zero, so all the power is sent to the battery. In CRUISE mode, due to reduced power demand of the train, the FC provides all the power of the train and charges the battery up to its power limit up to a SOC of 80%. If a braking event occurs in this condition, a ballast resistor and mechanical brakes are used to stop the train.

When battery's SOC reaches 20%, ACH is set to ON, i.e. the FC feeds the motor and the battery. This needs to be considered as a limp mode of the train, as the traction power is limited, being the maximum component of the motor q-axis current no larger than i_{q1max}. No operational differences exist in ACC and CRUISE modes, and the battery is charged every time the motor current is lower than the FC maximum current, i.e. at low speed and/or at low traction loads.

In DEC mode, regenerative braking is activated in the same way as when ACH is OFF, so the battery is charged with its maximum current. ACH mode remains ON until the battery's SOC has reached 35%, to enable a sufficient time before the ACH mode is activated again.

III. CASE STUDY: REPLACEMENT OF SOUTH WEST REGIONAL DIESEL TRAIN WITH HYDROGEN TRAIN

The suggested framework, incorporating the information from Table 1, has been substituted for the diesel engine

in the train route depicted in **Fig. 5**. This is a branch line approximately 6.7 km long and 5 stations located in the south west of the UK at St Ives. This branch line is currently operated with a British Rail Class 150 diesel multiple unit and the power requirements are compatible with the train in Table 1. The line is operated by a single unit, making 24 round trips per day, has 4 coaches and each has a 213kW diesel engines which correspond to 852 kW in total. Therefore, eight of the proposed traction modules are used to meet the power requirements of the adopted regional train.

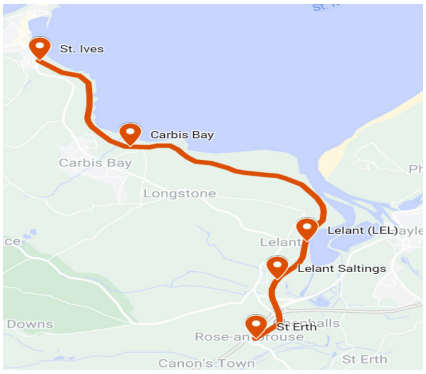

FIGURE 5. Line diagram of the St Ives branch.

In the conversion to a hydrogen train, the diesel engines have been replaced by eight 110kW AS-PMSMs to keep the same train performance. The FC and battery power ratings have been designed using the single-train simulator (STS) developed at the University of Birmingham [40] for a round-trip journey of 13.4 km that takes approximately 25 minutes, as shown in **Fig. 6**. FC is designed to provide the average power calculated by the STS (**Fig. 6a**) and divided by number of motors, resulting in a power of 30 kW per FC. The maximum power of each battery is instead 80 kW per motor and each peak has a duration of several tens of seconds, while the coasting occurs for periods of several minutes.

IV. EXPERIMENTAL VALIDATION OF THE PROPOSED ENERGY MANAGEMENT WITH HARDWARE IN THE LOOP

The proposed power-sharing scheme and motor control has been implemented on microcontroller Texas Instrument C2000 Delfino MCU F28379D and LaunchPad development kit for experimental verification using a hardware-in-the-loop (HIL) approach as zoomed view is given in **Fig.7**. This real-time HIL simulator allows the implementation of control loops, electrical machines and converters, and power plants, as well as precise measurement functions. It has two parts: the schematic editor, where the system is modelled, and HIL SCADA, where the results are displayed and analogue I/O implemented.

The block diagram of the complete traction unit and the HIL simulator, shown in **Fig. 8 and 9**, includes the AS-PMSM, the FC, the battery and the 2 voltage source converters. All controller blocks have been embedded in an external microcontroller to drive the motor in real time.

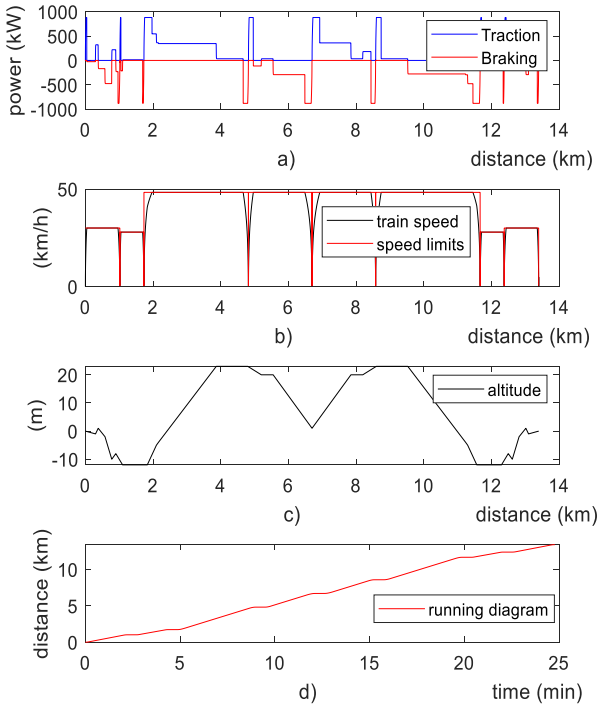

FIGURE 6. Simulation results for a round trip between St Erth - St Ives.

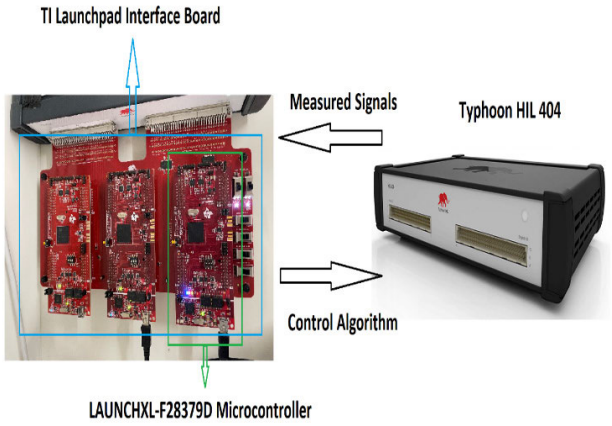

FIGURE 7. TyphoonHIL real-time simulator and microcontroller board.

The power sources, AS-PMSM and VSIs, have remained in the schematic panel after transferring the FOC with the power-sharing scheme to the microchip. The reference speed has been set equal to the speed limit on each specific part of the track and a maximum acceleration rate of 1 m/s^2 has been used for the train.

Fig. 10-a shows the train speed compared to the speed limit on the line and **Fig. 10-g** shows the distance travelled. The motor and resistant torques are shown in **Fig. 10-b**, showing an effective torque control limited at 850 Nm for both acceleration and braking. The resistant torque mainly depends on the track gradient shown in **Fig. 10-h** as the aerodynamic drag is not substantial due to the low speed on

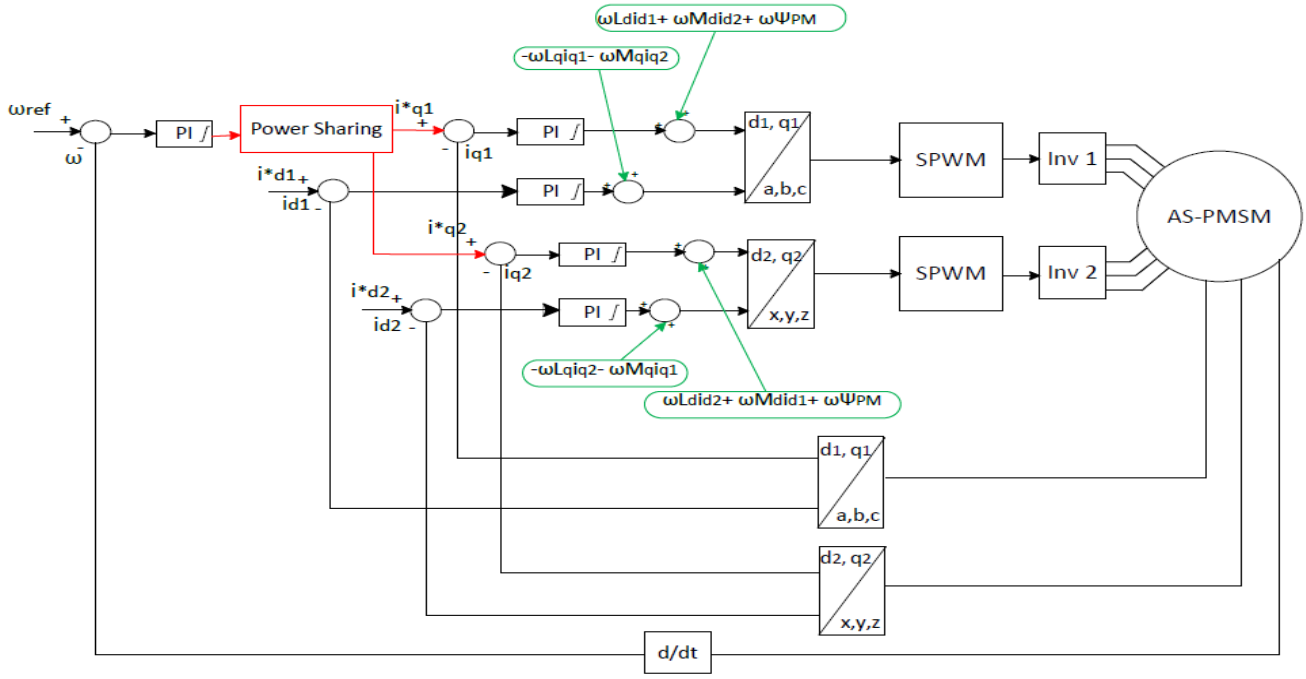

FIGURE 8. Complete view of the proposed system with motor control.

FIGURE 9. Typhoon HIL device and microcontroller board.

the line. It is worth noting that for this particular route there is no field-weakening, as the train speed is always lower than the base speed, so the current id is equal 0 and it is not shown in the results.

The battery's SOC is shown in **Fig. 10-f** and it can be seen that the SOC increases from 50% to approximately 67% at the end of the round-trip. This means that the ACH mode is never activated, as it should happen for normal operations. In fact, when ACH mode is active, the train would not be able to follow the timetable, as acceleration would be severely constrained by the absence of the battery's contribution. At minutes 5, FC and battery are both used to travel uphill when the train is in ACC mode and the battery's SOC is decreasing. At minute 10 the train travels uphill albeit at constant speed, so the CRUISE mode is active. Therefore, the FC supplies the train and also charges the battery. When the train stops shortly after, the control switches to DEC mode and the battery is also charged for a few more seconds. At minutes 6 and 17, the train travels downhill and DEC mode occurs for a longer period. The figure shows clearly that this situation is ideal for battery charging, as regenerative braking is activated with a top-up from the FC.

Fig. 10-c and **10-d** show the q-axis currents of FC and battery, respectively. According to the power sharing algorithm, the FC provide its maximum power during acceleration and cruising, while the battery supply the remainder to enable to motor to follow the torque profile. For example, at minute 6 the average values of iq1 and iq2 are 57.54 A and -45.27 A respectively, confirming that the FC charges the battery via the motor. The current of AS-PMSM is shown in **Fig. 10-e**, clearly evidencing that the two windings have different thermal load, as the RMS currents are 64 A and 137 A, respectively, confirming that special care needs to be devoted to the motor's winding design.

V. COMPARISON WITH THE STANDARD TOPOLOGY

This section compares the proposed traction system with the state-of-art configuration with boost DC-DC converters in terms of total volume, weight and the cost. A widely used converter topology is shown in **Fig. 11** and consists of 4 inductors, 1 capacitor, 12 IGBTs, 12 anti-parallel diodes (APDs), and 2 diodes (Ds). The proposed converter has the same number of IGBTs with one diode, but no capacitors and inductors. On the other hand, the standard topology provides a regulated DC voltage for the motor drive that simplifies machine control.

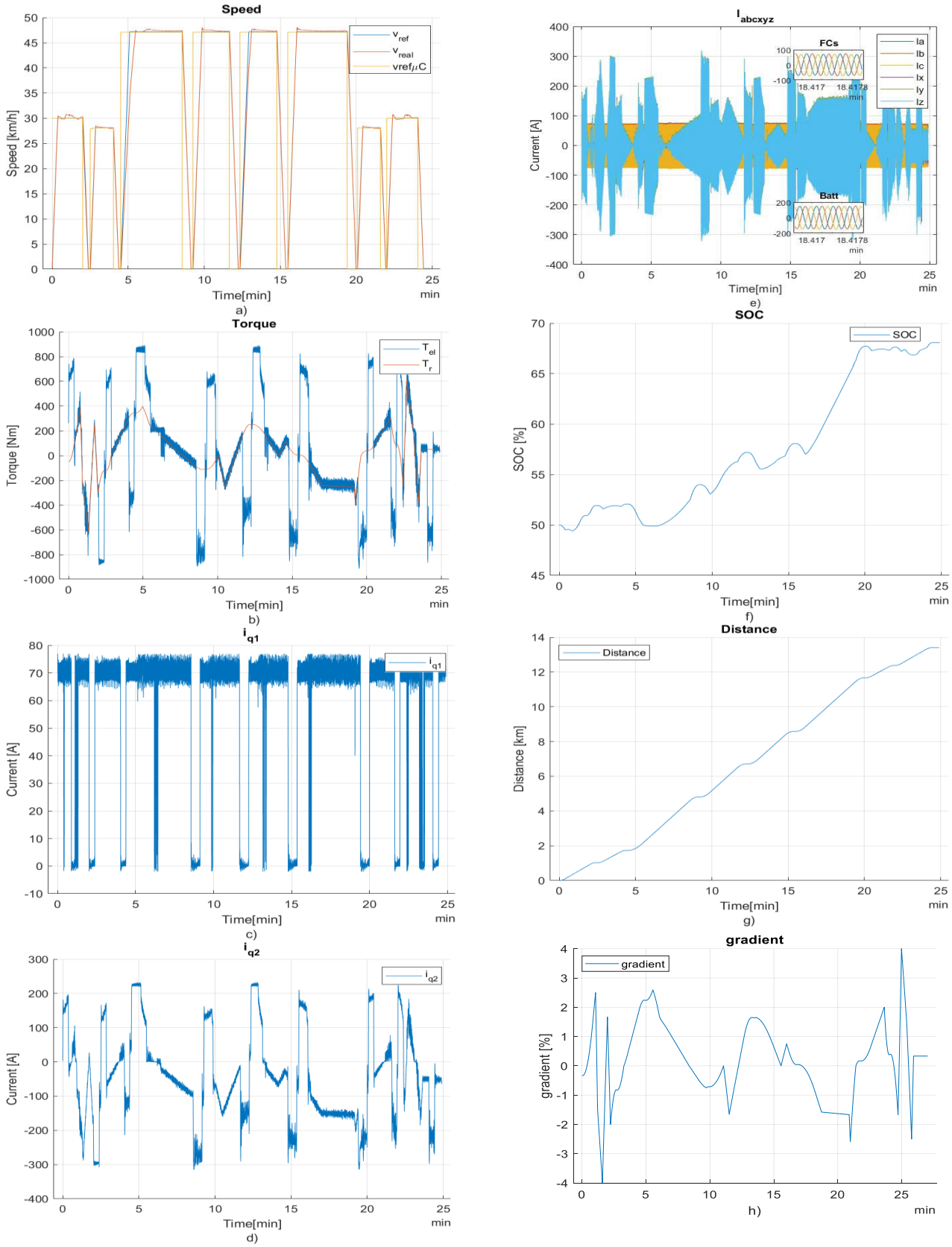

FIGURE 10. HIL simulation result: train speed (a), motor and resistant torques (b), FC current (c), battery current (d), motor current (e), battery's SOC (f), distance travelled by the trains with stations (g), track's gradient (h).

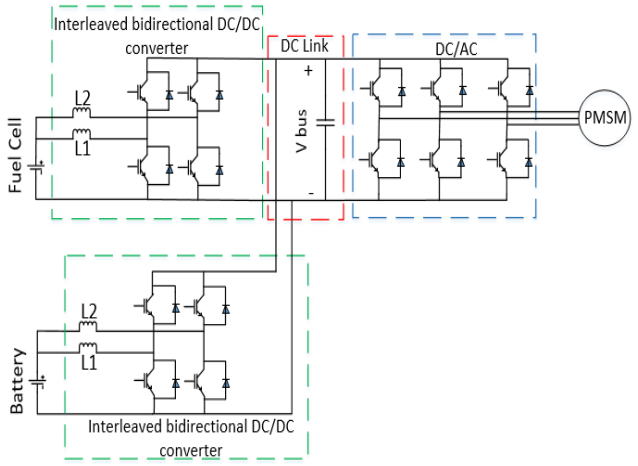

FIGURE 11. Standard interleaved converter architecture.

The energy density of capacitors, power inductors, as well as apparent power of diodes and IGBTs have been taken from the datasheets of commercial products. To simplify the comparison procedure, the converters are assumed to be lossless.

A. APPARENT POWER OF SEMICONDUCTOR DEVICES

The apparent power requirements of semiconductor devices are investigated and compared for both topologies. Voltage levels of power sources are higher in the proposed traction system, due to the absence of DC-DC boost converters. The input voltages of the DC-DC converters have been chosen to 500 V, while the DC-bus voltage has been kept at 750 V like the original train.

1) STANDARD INTERLEAVED CONVERTER ARCHITECTURE

The interleaved boost converters are designed for the power of the FC and battery respectively, whereas the inverter is designed to meet the peak machine current. As in the proposed control algorithm, FC and battery share the power in the same proportion. Based on the input voltages and powers the input currents are 60 A for the FC and 180 A for the battery. Therefore, choosing available devices to meet the minimum requirements (SKM75GB12F4), for the FC's DC-DC converters the following results are obtained:

$$\begin{aligned} S_{FC} &= 2V_{IGBT}I_{IGBT} + 2V_{AP}I_{APD} + 2V_{D}I_{D} \\ &== 2 \times 1,200 \times 75 + 2 \\ &\quad \times 1,200 \times 75 + 2 \times 1,200 \times 75 = 0.54\text{MVA} \end{aligned} \quad (1)$$

Similarly using SKM200GB12E4 for the battery's converter, the result is:

$$\begin{aligned} S_{Battery} &= 4V_{IGBT}I_{IGBT} + 4V_{APD}I_{APD} \\ &== 4 \times 1,200 \times 200 + 4 \\ &\quad \times 1,200 \times 200 = 1.92\text{MVA} \end{aligned} \quad (2)$$

For the inverter the peak value of the rated motor current is 270 A (191A RMS) and, using SEMiX303GD12E4c, the total apparent power is:

$$\begin{aligned} S_{Inverter} &= 6V_{IGBT}I_{IGBT} + 6V_{APD}I_{APD} == 6 \times 1,200 \\ &\quad \times 300 + 6 \times 1,200 \times 300 = 4.32\text{MVA} \end{aligned} \quad (3)$$

Leading to a total apparent power of the state-of-the-art topology of 6.78 MVA.

2) PROPOSED TOPOLOGY

The power devices of the proposed configuration are also designed to meet the peak machine current. For the FC converter, SEMiX151GD12E4s is suitable for the IGBTs and the anti-parallel diodes [41]. For the series diode, it has been considered that the maximum difference between the FC voltage and the DC-link voltage is 250 V as indicated in Table 1. Therefore, the apparent power of the FC inverter is:

$$\begin{aligned} S_{FC} &= 6V_{IGBT}I_{IGBT} + 6V_{APD}I_{APD} \\ &\quad + V_{D}I_{D} == 6 \times 1,200 \times 75 + 6 \\ &\quad \times 1,200 \times 75 + 300 \times 60 = 1.10\text{MVA} \end{aligned} \quad (4)$$

For the battery, the module SKM600GB126D is instead used and the apparent power of the inverter is:

$$\begin{aligned} S_{Battery} &= 6V_{IGBT}I_{IGBT} + 6V_{APD}I_{APD} \\ &== 6 \times 1,200 \times 300 + 6 \times 1,200 \\ &\quad \times 300 = 4.32\text{MVA} \end{aligned} \quad (5)$$

Finally, the total apparent power of the proposed converter is equal to 5.42 MVA, which is 20% lower than the traditional topology.

B. ENERGY OF INDUCTORS (STANDARD TOPOLOGY ONLY)

For the traditional topology, the current ripple Δi_L has been chosen to 20% of the dc current at peak power. The inductor values for the FC and battery DC-DC converters are:

$$\begin{aligned} L_{fc} &= \frac{V_{dc}\,(1-D)\,D}{f_s N I_{fc} \Delta i_L} \\ &= \frac{750 \times \frac{2}{9}}{10,000 \times 2 \times 60 \times 0.2} = 694\mu\text{H} \end{aligned} \quad (6)$$

$$\begin{aligned} L_{b} &= \frac{V_{dc}\,(1-D)\,D}{f_s N I_{b} \Delta I_L} \\ &= \frac{750 \times \frac{2}{9}}{10,000 \times 2 \times 180 \times 0.2} = 231\mu\text{H} \end{aligned} \quad (7)$$

where N is number of interleaved legs, equal to 2, f_s is the switching frequency, selected at 10 kHz, and D is the duty cycle equal to 1/3 when the FC and the battery voltage are at their lowest values. These inductors store the following energies:

$$W_{Lfc} = \frac{1}{2}L_{fc}I_{fc}^2 = 0.5 \times 694 \times 10^{-6} \times 60^2 = 1.25\text{J} \quad (8)$$

$$W_{Lb} = \frac{1}{2}L_{b}I_{b}^2 = 0.5 \times 231 \times 10^{-6} \times 180^2 = 3.74\text{J} \quad (9)$$

Leading to a total inductor energy of 4.99 J. Using for example power inductors RD8127-64-0M8 [42] and CH-200 [43] for FC and battery respectively, the total volume and weight of the inductors are 12 dm^3 and 44 kg, respectively. For the proposed topology, there are no inductors in the system, so this energy is not required.

C. ENERGY OF CAPACITORS

1) STANDARD INTERLEAVED CONVERTER ARCHITECTURE

For the traditional topology the only capacitor needed is at the dc-link. If the voltage ripple Δv_{dc} is designed at 1% of the average voltage, the capacitor value for the DC-link is:

$$C = \frac{P_{dc}}{f_s N V_{dc}^2 \Delta v_{dc}} \frac{D}{1-D} = \frac{118,000 \times \frac{1}{2}}{10,000 \times 2 \times 750^2 \times 0.01} = 524\mu F \quad (10)$$

where P_{dc} is the power of the inverter, N is the number of interleaved legs, equal to 2, f_s is the switching frequency, assumed the same as the DC-DC converters. This capacitor stores the following energy:

$$W_C = \frac{1}{2} C V_{dc}^2 = 0.5 \times 524 \times 10^{-6} \times 750^2 = 147J \quad (11)$$

Using for example EZPV1B406MTS [44] as a capacitor bank by connecting like 14 of them in series to have sufficient capacitance value for the converter, the volume and weight of capacitor are 2 dm^3 and 2 kg, respectively.

2) PROPOSED CONVERTER TOPOLOGY

In the proposed topology, each inverter requires a high-frequency capacitor to smooth the current of the FC and the battery, which is recommended to reduce thermal stresses and increase components' lifetime. The peak current of the capacitors is given by the following equation [45]:

$$I_C = I_n \sqrt{2M \left[\frac{\sqrt{3}}{4\pi} + \cos^2 \varphi \left(\frac{\sqrt{3}}{\pi} - \frac{9}{16} M \right) \right]} \quad (12)$$

where M is the inverter modulation index and $\cos\varphi$ is the load power factor. Assuming for both inverters' M values change between 1 and 0, while $\cos\varphi$ varies between 0.93 and 0.98 for this particular motor. Based on the worst-case scenario, it was chosen $M = 0.5$ and $\cos\varphi = 0.98$, and the maximum current of the capacitor for the FC and the battery are 44 A and 126 A, respectively. The capacitance is given by:

$$C = \frac{I_C}{f_s V_{dc} \Delta v_{dc}} \frac{D}{1-D} \quad (13)$$

Assuming $V_{dc} = 500$ V for both FC and battery, the capacitances are $C_{fc} = 440\,\mu$F and $C_b = 1{,}260\,\mu$F. Therefore, the energies stored by these capacitors are:

$$W_{Cfc} = \frac{1}{2} C_{fc} V_{fc}^2 = 0.5 \times 440 \times 10^{-6} \times 750^2 = 124J \quad (14)$$

TABLE 2. Comparison chart of two schematics.

	Standard converter	Proposed converter
No. of IGBT modules	12	12
IGBT Rating (kVA)	6,600	5,400
IGBT Volume (dm^3)	820	720
IGBT Weight (kg)	2	1
IGBT Cost (£)	£1,872	£983
No. of diodes	2	1
Diode Rating (kVA)	180	18
Diode Volume (dm^3)	3	2
Diode Weight (kg)	0.1	0.1
Diode Cost (£)	£11	£7
Number of Capacitors	1	2
Capacitor Volume (dm^3)	2	5
Capacitor Weight (kg)	2	6
Capacitor Cost (£)	£214	£588
Number of Inductors	4	0
Inductor Volume (dm^3)	12	0
Inductor Weight (kg)	44	0
Inductor Cost (£)	£787	0

$$W_{Cb} = \frac{1}{2} C_b V_b^2 = 0.5 \times 1,260 \times 10^{-6} \times 750^2 = 354J \quad (15)$$

leading to a total stored energy of 478 J. Choosing EZPV1B406MTS, volume and mass of the capacitors are 1 dm^3 and 2 kg for the FC and 4 dm^3 and 4 kg for the battery.

The results for the two converter topologies are summarised in **Table 2**. The proposed converter has a significantly lower cost, weight and lower volume and apparent power of the converters, but this must be traded off against a more complex control logic and the need of compensating the voltage drops of FCs and batteries with a higher rated voltage. Also, the motor is more expensive and more complex. Finally, the cost of the power semiconductors almost one half and the energy storage is nearly doubled of the traditional converter.

VI. CONCLUSION

This paper has presented a new traction system for hydrogen trains based on asymmetrical 6-phase permanent magnet synchronous motors. For each motor, the 2 set of three phase windings have been supplied by 2 traction inverter connected to the FC and the battery, respectively. This configuration allows the removal of the DC-DC boost converters used in traditional traction systems, increasing significantly the power density of the motor drive and reducing cost. To enable satisfactory motor control, the power sources must be designed with a voltage higher than traditional system to cope with their voltage drop when the motor accelerates. The motor provides an electromagnetic coupling between the FC and the battery, allowing charging at low traction load and every time the train is braking, either for stopping or because it travels downhill. Charging is also possible when the train is stationary, because the direct and quadrature components of the 2 inverters can be controlled independently.

The proposed traction system has been designed for a case of a regional line in the UK to replace an existing diesel train, and studied with a hardware-in-the-loop approach to

verify the power sharing performance and the capability of charging the battery for different conditions of velocity and traction load. The results show good performance of the traction drive with no negative effect on the vector control due to the voltage drop of the FC and the battery during train's acceleration. Also, the battery charging is effective and activated as predicted by the theoretical analysis. The paper has then undertaken a comparison with the most common traction system for hydrogen train, showing a reduction of the total apparent power of the converters of 20%, a reduction of volume and weight of energy storage devices of 14% and 85% respectively, and a decrease of cost of the basic components by 45% because of removal of inductors which is costly and bulky, from power converter unit.

This research is focused on the design and control of a AS-PMSM that is independently supplied with hydrogen and battery light railway applications, as indicated in the introduction. Following a successful practical implementation, the vehicle's traction side reliability will increase, and user expectations will be somewhat better fulfilled. This feature of multiphase machines is generic and would be covered for future works in a detail way. Because of this property, feeding each phase group separately will result in fault tolerance. This also improves the system's reliability with multisource power converter units which are available for multiphase structures. A few recommended architectures also support these converter topologies to enable fault-tolerant operation and voltage drop compensation in the literature.

REFERENCES

[1] J. Lee, J. Jo, S. Choi, and S. Han, "A 10-kW SOFC low-voltage battery hybrid power conditioning system for residential use," *IEEE Trans. Energy Convers.*, vol. 21, no. 2, pp. 575–585, Jun. 2006.

[2] X. Yu, M. R. Starke, L. M. Tolbert, and B. Ozpineci, "Fuel cell power conditioning for electric power applications: A summary," *IET Electr. Power Appl.*, vol. 1, no. 5, pp. 643–656, 2007.

[3] A. V.-Blanco, C. Aguilar-Castillo, F. C.-Abarca, and J. Arau-Roffie, "Two-stage and integrated fuel cell power conditioner: Performance comparison," in *Proc. IEEE APEC*, Feb. 2009, pp. 452–458.

[4] L. S. Xavier, W. C. S. Amorim, A. F. Cupertino, V. F. Mendes, W. C. do Boaventura, and H. A. Pereira, "Power converters for battery energy storage systems connected to medium voltage systems: A comprehensive review," *BMC Energy*, vol. 1, no. 1, pp. 1–15, Dec. 2019.

[5] *Ultracapacitor Applications for Uninterruptible Power Supplies (Ups)*, Skeleton Technologies GmbH, Großröhrsdorf, Berlin, Germany, 2017.

[6] F. Naseri, E. Farjah, and T. Ghanbari, "An efficient regenerative braking system based on battery/supercapacitor for electric, hybrid, and plug-in hybrid electric vehicles with BLDC motor," *IEEE Trans. Veh. Technol.*, vol. 66, no. 5, pp. 3724–3738, May 2017.

[7] S. Campanari, G. Manzolini, and F. Garcia de la Iglesia, "Energy analysis of electric vehicles using batteries or fuel cells through well-to-wheel driving cycle simulations," *J. Power Sources*, vol. 186, no. 2, pp. 464–477, Jan. 2009.

[8] W. Gao, "Performance comparison of a fuel cell-battery hybrid powertrain and a fuel cell-ultracapacitor hybrid powertrain," *IEEE Trans. Veh. Technol.*, vol. 54, no. 3, pp. 846–855, May 2005.

[9] T. Azib, O. Bethoux, G. Remy, C. Marchand, and E. Berthelot, "An innovative control strategy of a single converter for hybrid fuel cell/supercapacitor power source," *IEEE Trans. Ind. Electron.*, vol. 57, no. 12, pp. 4024–4031, Dec. 2010.

[10] G. Dotelli, R. Ferrero, P. Gallo Stampino, S. Latorrata, and S. Toscani, "Supercapacitor sizing for fast power dips in a hybrid supercapacitor—PEM fuel cell system," *IEEE Trans. Instrum. Meas.*, vol. 65, no. 10, pp. 2196–2203, Oct. 2016.

[11] A. Rujas, V. M. López, A. García-Bediaga, A. Berasategi, and T. Nieva, "Influence of SiC technology in a railway traction DC–DC converter design evolution," in *Proc. IEEE Energy Convers. Congr. Expo. (ECCE)*, Oct. 2017, pp. 931–938.

[12] S. E. Schulz, "Exploring the high-power inverter: Reviewing critical design elements for electric vehicle applications," *IEEE Electrific. Mag.*, vol. 5, no. 1, pp. 28–35, Mar. 2017.

[13] R. Burkart and J. W. Kolar, "Component cost models for multi-objective optimizations of switched-mode power converters," in *Proc. IEEE Energy Convers. Congr. Expo.*, Sep. 2013, pp. 2139–2146.

[14] H.-B. Shin, J.-G. Park, S.-K. Chung, H.-W. Lee, and T. A. Lipo, "Generalised steady-state analysis of multiphase interleaved boost converter with coupled inductors," *IEE Proc.-Electric Power Appl.*, vol. 152, no. 3, p. 584, 2005.

[15] R. R. de Melo, F. L. Tofoli, S. Daher, and F. L. M. Antunes, "Interleaved bidirectional DC–DC converter for electric vehicle applications based on multiple energy storage devices," *Electr. Eng.*, vol. 102, no. 4, pp. 2011–2023, Dec. 2020.

[16] S. Chakraborty, H.-N. Vu, M. M. Hasan, D.-D. Tran, M. E. Baghdadi, and O. Hegazy, "DC–DC converter topologies for electric vehicles, plug-in hybrid electric vehicles and fast charging stations: State of the art and future trends," *Energies*, vol. 12, no. 8, p. 1569, Apr. 2019.

[17] O. Salari, M. Nouri, K. H. Zaad, A. Bakhshai, and P. Jain, "A multi-source inverter for electric drive vehicles," in *Proc. IEEE Energy Convers. Congr. Expo. (ECCE)*, Sep. 2018, pp. 3872–3879.

[18] L. Dorn-Gomba, E. Chemali, and A. Emadi, "A novel hybrid energy storage system using the multi-source inverter," in *Proc. IEEE Appl. Power Electron. Conf. Expo. (APEC)*, San Antonio, TX, USA, Mar. 2018, pp. 684–691.

[19] M. Jang and V. G. Agelidis, "A minimum power-processing-stage fuel-cell energy system based on a boost-inverter with a bidirectional backup battery storage," *IEEE Trans. Power Electron.*, vol. 26, no. 5, pp. 1568–1577, May 2011.

[20] X. Sun, C. Hu, J. Zhu, S. Wang, W. Zhou, Z. Yang, G. Lei, K. Li, B. Zhu, and Y. Guo, "MPTC for PMSMs of EVs with multi-motor driven system considering optimal energy allocation," *IEEE Trans. Magn.*, vol. 55, no. 7, pp. 1–6, Jul. 2019.

[21] K. Matsuoka and M. Kondo, "Energy saving technologies for railway traction motors," *IEEJ Trans. Electr. Electron. Eng.*, vol. 5, no. 3, pp. 278–284, May 2010.

[22] K. Kondo, "Recent energy saving technologies on railway traction systems," *IEEJ Trans. Electr. Electron. Eng.*, vol. 5, no. 3, pp. 298–303, May 2010.

[23] G. Valente, L. Papini, A. Formentini, C. Gerada, and P. Zanchetta, "Open-circuit fault tolerant study of bearingless multi-sector permanent magnet machines," in *Proc. Int. Power Electron. Conf.*, May 2018, pp. 4034–4041.

[24] H. S. Che and W. P. Hew, "Dual three-phase operation of single neutral symmetrical six-phase machine for improved performance," in *Proc. 41st Annu. Conf. IEEE Ind. Electron. Soc.*, Nov. 2015, pp. 001176–001181.

[25] K. S. Khan, W. M. Arshad, and S. Kanerva, "On performance figures of multiphase machines," in *Proc. 18th Int. Conf. Electr. Mach.*, Sep. 2008, pp. 1–5.

[26] W. N. W. A. Munim, M. J. Duran, H. S. Che, M. Bermudez, I. González-Prieto, and N. A. Rahim, "A unified analysis of the fault tolerance capability in six-phase induction motor drives," *IEEE Trans. Power Electron.*, vol. 32, no. 10, pp. 7824–7836, Oct. 2017.

[27] R. Nelson and P. Krause, "Induction machine analysis for arbitrary displacement between multiple winding sets," *IEEE Trans. Power App. Syst.*, vol. PAS-93, no. 3, pp. 841–848, May 1974.

[28] K. S. Khan, *Comparative Analysis of Multiphase Machines*. Göteborg, Sweden: Chalmers Univ., 2008.

[29] X. Wang, Z. Wang, M. Cheng, and Y. Hu, "Remedial strategies of T-NPC three-level asymmetric six-phase PMSM drives based on SVM-DTC," *IEEE Trans. Ind. Electron.*, vol. 64, no. 9, pp. 6841–6853, Sep. 2017.

[30] Z. Wang, B. Zhang, Y. Wang, Y. Zhang, and M. Cheng, "Analysis and control of active neutral-point-clamping three-level inverters under fault tolerant operation modes," in *Proc. 18th Int. Conf. Electr. Mach. Syst. (ICEMS)*, Oct. 2015, pp. 2140–2146.

[31] M. B. D. R. Correa, C. B. Jacobina, E. R. C. da Silva, and A. M. N. Lima, "A general PWM strategy for four-switch three-phase inverters," *IEEE Trans. Power Electron.*, vol. 21, no. 6, pp. 1618–1627, Nov. 2006.

[32] E. Levi, "Multiphase electrical machines for variable-speed applications," *IEEE Trans. Ind. Electron.*, vol. 55, no. 5, pp. 1893–1909, May 2008.

[33] J. Karttunen, S. Kallio, J. Honkanen, P. Peltoniemi, and P. Silventoinen, "Stability and performance of current harmonic controllers for multiphase PMSMs," *Control Eng. Pract.*, vol. 65, pp. 59–69, Aug. 2017.
[34] Y. Hu, Z.-Q. Zhu, and K. Liu, "Current control for dual three-phase permanent magnet synchronous motors accounting for current unbalance and harmonics," *IEEE J. Emerg. Sel. Topics Power Electron.*, vol. 2, no. 2, pp. 272–284, Jun. 2014.
[35] A. Tessarolo and C. Bassi, "Stator harmonic currents in VSI-fed synchronous motors with multiple three-phase armature windings," *IEEE Trans. Energy Convers.*, vol. 25, no. 4, pp. 974–982, Dec. 2010.
[36] S. H. F. Yua, "A hybrid current controller for dual three-phase permanent magnet synchronous motors," *IEEJ Trans. Electr. Electron. Eng.*, vol. 9, pp. 214–218, Mar. 2014.
[37] N. Polater and P. Tricoli, "Technical review of traction drive systems for light railways," *Energies*, vol. 15, no. 9, p. 3187, Apr. 2022.
[38] N. Polater, T. Kamel, and P. Tricoli, "Control and power sharing strategy of dual three-phase permanent magnet synchronous motor for light railway applications," in *Proc. IEEE Vehicle Power Propuls. Conf. (VPPC)*, Gijon, Spain, Oct. 2021, pp. 1–6.
[39] S. Hillmansenn, *Single Train Simulator, Birmingham Center for Railway Research and Education*. Birmingham, U.K.: Univ. Birmingham.
[40] (1951). *Semikron*. Accessed: Jul. 29, 2022. [Online]. Available: https://www.semikron.com/products/product-classes/igbt-modules.html
[41] *Mouser Electronics*. Accessed: Feb. 8, 2023. [Online]. Available: https://eu.mouser.com/datasheet/2/355/RDseries-3001103.pdf
[42] CC Series. Accessed: Feb. 8, 2023. [Online]. Available: https://www.digikey.com/en/products/detail/signal-transformer/CH-200/1984836
[43] (1939). *Farnell*. Accessed: Mar. 20, 2023. [Online]. Available: https://uk.farnell.com/panasonic/ezpv1b406mts/cap-40uf-1-1kv-film-radial/dp/3373096?pf_custSiteRedirect=true
[44] *Specter Engineering*. Accessed: Mar. 4, 2023. [Online]. Available: https://www.specterengineering.com/blog/2019/9/7/dc-link-capacitor-selection-for-your-inverter
[45] V. M. GmbH. *Permanent Magnet Synchronous Motors for Inverter Operation*. Accessed: Mar. 5, 2023. [Online]. Available: https://www.vem-group.com/fileadmin/content/pdf/Download/Kataloge/Kataloge/pm_en.pdf

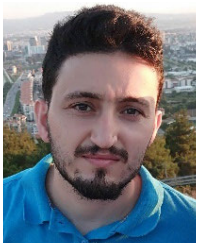

NURSAID POLATER was born in Van, Turkey, in 1991. He received the B.Sc. degree in electrical engineering from Yıldız Technical University, Turkey, in 2014, the M.Sc. degree in electrical engineering for renewable and sustainable energy from the University of Nottingham, U.K., in 2017, and the Ph.D. degree from the Department of Electronic, Electrical and Systems Engineering, University of Birmingham, U.K., in 2023. He is currently an Assistant Professor with the Department of Electrical Electronic Engineering, Yozgat Bozok University, Yozgat, Turkey. His research interests include electric machines, drives and power electronics, multi-phase permanent magnet synchronous motors, and the modeling and control of renewable hybrid traction systems for electric vehicles. He is a member of the Birmingham Centre for Railway Research and Education (BCRRE).

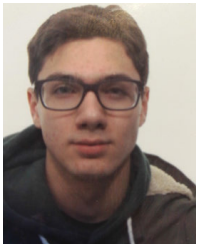

FRANCESCO MAGGIULLI was born in Bergamo, Italy, in 1998. He received the B.Sc. degree in electrical engineering from Politecnico di Milano, Italy, in 2020, where he is currently pursuing the M.Sc. degree in electrical engineering.

He has undertaken the M.Sc. thesis as a Visitor Post-Graduate Student with the Birmingham Centre for Railway Research and Education (BCRRE), University of Birmingham. His research interests include electrical drives, power electronics, microcontrollers, and traction systems for electric vehicles.

GIOVANNI MARIA FOGLIA received the M.S. and Ph.D. degrees in electrical engineering from Politecnico di Milano, Milano, Italy, in 1997 and 2000, respectively.

He is currently an Assistant Professor with the Department of Energy, Politecnico di Milano. His research interests include electric machines, drives and power electronics, and the analysis and design of permanent magnet electrical machines, with a focus on modular axial flux PM synchronous machines for wind energy conversion systems.

PIETRO TRICOLI (Senior Member, IEEE) was born in Naples, Italy, in September 1978. He received the M.S. (cum laude) and Ph.D. degrees in electrical engineering from the University of Naples Federico II, Naples, in 2002 and 2005, respectively.

He was a Visiting Scholar with the Department of Electrical and Computer Engineering, University of Wisconsin–Madison, Madison, WI, USA, in 2005. In 2006, he was a Visiting Scholar with the Department of Electrical and Electronic Engineering, Nagasaki University, Nagasaki, Japan. From 2006 to 2011, he was a Postdoctoral Research Fellow with the Department of Electrical Engineering, University of Naples Federico II. In 2011, he was a Lecturer with the Department of Electronic, Electrical, and Systems Engineering, University of Birmingham, Birmingham, U.K., where he was a Senior Lecturer, in 2017, and a Reader in power electronics systems, in 2021. He has authored more than 100 scientific papers published in international journals and conference proceedings. His research interests include storage devices for road electric vehicles railways, rapid transit systems, wind and photovoltaic generation, railway electrification systems, and modeling and control of multilevel converters.

Dr. Tricoli is a member of the IEEE Industrial Electronics Society and the Energy Institute. He is the Web and Publication Chair of the International Conference on Clean Electrical Power. He is the Deputy Editor-in-Chief of *IET Journal Renewable Power Generation*. He is a Registered Professional Engineer in Italy.